ResearchGate

See discussions, stats, and author profiles for this publication at: https://www.researchgate.net/publication/282362490

1730 ftp

DATASET · OCTOBER 2015

READS
20

8 AUTHORS, INCLUDING:

Klas Gunnarsson
Uppsala University
50 PUBLICATIONS **657** CITATIONS
SEE PROFILE

Peter Svedlindh
Uppsala University
279 PUBLICATIONS **5,491** CITATIONS
SEE PROFILE

All in-text references underlined in blue are linked to publications on ResearchGate, letting you access and read them immediately.

Available from: Sven Oscarsson
Retrieved on: 02 February 2016

ADVANCED MATERIALS

Experimental

Characterization: The UV-visible spectra were recorded on a Shimadzu 3101 spectrophotometer. Dynamic light scattering studies were carried out using a Horiba LB-550 instrument. Transmission electron micrographs of the clusters were recorded by applying a drop of the sample to a carbon-coated copper grid (JEOL JEM-200CX). AFM measurements were obtained using a Digital Nanoscope III in the tapping mode.

Photoelectrochemical Measurements: The photoelectrochemical measurements were performed in a one-compartment Pyrex UV cell with a standard three electrode arrangement consisting of a working electrode, a Pt wire counter electrode, and a $Ag/AgNO_3$ reference electrode (0.5 M LiI and 0.01 M I_2 in acetonitrile as the electrolyte). Photocurrent measurements were made with an ALS 630A electrochemical analyzer. Monochromatic light obtained by passing light from a 500 W xenon lamp (Ushio XB-50101AA-A) through a monochromator (Ritsu MC-10N) was used for excitation.

Received: October 28, 2004
Final version: March 11, 2005
Published online: May 12, 2005

[1] A. Hagfeldt, M. Grätzel, *Acc. Chem. Res.* **2000**, *33*, 269.
[2] N. Hirata, J.-J. Lagref, E. J. Palomares, J. R. Durrant, M. K. Nazeeruddin, M. Grätzel, D. Di Censo, *Chem. Eur. J.* **2004**, *10*, 595.
[3] a) G. Yu, J. Gao, J. C. Hummelen, F. Wudl, A. J. Heeger, *Science* **1995**, *270*, 1789. b) F. Padinger, R. S. Rittberger, N. S. Sariciftci, *Adv. Funct. Mater.* **2003**, *13*, 85. c) M. M. Wienk, J. M. Kroon, W. J. H. Verhees, J. Knol, J. C. Hummelen, P. A. van Hal, R. A. J. Janssen, *Angew. Chem. Int. Ed.* **2003**, *42*, 3371.
[4] a) J. J. M. Halls, C. A. Walsh, N. C. Greenham, E. A. Marseglia, R. H. Friend, S. C. Moratti, A. B. Holmes, *Nature* **1995**, *376*, 498. b) L. Schmidt-Mende, A. Fechtenkötter, K. Müllen, E. Moons, R. H. Friend, J. D. MacKenzie, *Science* **2001**, *293*, 1119. c) W. U. Huynh, J. J. Dittmer, A. P. Alivisatos, *Science* **2002**, *295*, 2425. d) J.-F. Nierengarten, *New J. Chem.* **2004**, *28*, 1177.
[5] a) D. R. Evans, N. L. P. Fackler, Z. Xie, C. E. F. Rickard, P. D. W. Boyd, C. A. Reed, *J. Am. Chem. Soc.* **1999**, *121*, 8466. b) K. Tashiro, T. Aida, J.-Y. Zheng, K. Kinbara, K. Saigo, S. Sakamoto, K. Yamaguchi, *J. Am. Chem. Soc.* **1999**, *121*, 9477.
[6] M. Shirakawa, N. Fujita, S. Shinkai, *J. Am. Chem. Soc.* **2003**, *125*, 9902.
[7] a) H. Imahori, *Org. Biomol. Chem.* **2004**, *2*, 1425. b) H. Imahori, S. Fukuzumi, *Adv. Funct. Mater.* **2004**, *14*, 525. c) H. Imahori, *J. Phys. Chem. B* **2004**, *108*, 6130.
[8] a) D. Gust, T. A. Moore, A. L. Moore, *Acc. Chem. Res.* **2001**, *34*, 40. b) S. Fukuzumi, D. M. Guldi, in *Electron Transfer in Chemistry*, Vol. 2 (Ed: V. Balzani), VCH, Weinheim **2001**, pp. 270–337.
[9] a) T. Hasobe, H. Imahori, S. Fukuzumi, P. V. Kamat, *J. Phys. Chem. B* **2003**, *107*, 12105. b) T. Hasobe, Y. Kashiwagi, M. A. Absalom, J. Sly, K. Hosomizu, M. J. Crossley, H. Imahori, P. V. Kamat, S. Fukuzumi, *Adv. Mater.* **2004**, *16*, 975.
[10] a) T. Hasobe, H. Imahori, P. V. Kamat, S. Fukuzumi, *J. Am. Chem. Soc.* **2003**, *125*, 14962. b) T. Hasobe, H. Imahori, P. V. Kamat, T. K. Ahn, S. K. Kim, D. Kim, A. Fujimoto, T. Hirakawa, S. Fukuzumi, *J. Am. Chem. Soc.* **2005**, *127*, 1216.
[11] a) H. Imahori, M. Arimura, T. Hanada, Y. Nishimura, I. Yamazaki, Y. Sakata, S. Fukuzumi, *J. Am. Chem. Soc.* **2001**, *123*, 335. b) H. Imahori, Y. Kashiwagi, Y. Endo, T. Hanada, Y. Nishimura, I. Yamazaki, Y. Araki, O. Ito, S. Fukuzumi, *Langmuir* **2004**, *20*, 73.
[12] P. V. Kamat, S. Barazzouk, S. Hotchandani, K. G. Thomas, *Chem. Eur. J.* **2000**, *6*, 3914.
[13] H. Imahori, N. V. Tkachenko, V. Vehmanen, K. Tamaki, H. Lemmetyinen, Y. Sakata, S. Fukuzumi, *J. Phys. Chem. A* **2001**, *105*, 1750.

Programmable Motion and Separation of Single Magnetic Particles on Patterned Magnetic Surfaces**

By *Klas Gunnarsson*,* *Pierre E. Roy*, *Solveig Felton*, *Johan Pihl*, *Peter Svedlindh*, *Simon Berner*, *Hans Lidbaum*, and *Sven Oscarsson*

Magnetic separation in heterogeneous suspensions is a well-established technique in life sciences. Magnetic particles (beads) with functionalized surfaces bind selectively to specific targets and can be separated from the suspension using an external magnetic field.[1] Thus, the particles and, hence, the target are separated as an entire group. Systems that enable controlled movement and positioning of single magnetic particles would open up new possibilities, e.g., handling small volumes or performing sophisticated sorting of different targets attached to different particles.

In this communication, a method for programmable motion and separation of single magnetic particles on a patterned magnetic surface is presented. The movement of micrometer-sized particles is controlled by an external, rotating magnetic field. Patterns of thin-film magnetic elements are tailored to form *transport lines* for magnetic particles. Junctions added to such transport lines allow separation of single magnetic particles. This method has the potential of improving a number of existing applications in biotechnology, such as the transportation and sorting of biological molecules on surfaces.

Magnetic particles in a homogeneous magnetic field show no translational motion. Assemblies of current-carrying wires is one approach to creating inhomogeneous magnetic fields.[2,3] With this technique, displacement of single magnetic particles has been achieved.[2] In another approach, inhomogeneities in the magnetic field are created by means of magnetic elements on a surface. Such inhomogeneities can be

[*] Dr. K. Gunnarsson, P. E. Roy, S. Felton, J. Pihl, Prof. P. Svedlindh
Department of Engineering Sciences, Uppsala University
Box 534, SE-751 21 Uppsala (Sweden)
E-mail: klas.gunnarsson@angstrom.uu.se
Dr. S. Berner, H. Lidbaum
Department of Surface Biotechnology, Uppsala University
Box 577, SE-751 23 Uppsala (Sweden)
Prof. S. Oscarsson
Department of Surface Biotechnology, Uppsala University
Box 577, SE-751 23 Uppsala (Sweden)
Prof. S. Oscarsson
Department of Chemical Engineering, Mälardalen University
Box 325, SE-631 05 Eskilstuna (Sweden)

[**] The authors thank Greger Ledung for fruitful discussions, and Lina Illiminsky is acknowledged for construction of the electromagnets used in this work. This work was supported by the Swedish Research Council and the Swedish Foundation for Strategic Research. Supporting Information is available online from Wiley InterScience or from the author.

 © 2005 WILEY-VCH Verlag GmbH & Co. KGaA, Weinheim DOI: 10.1002/adma.200401880

used to attract and trap particles to the elements. An external magnetic field is suitable for magnetizing the magnetic elements of the patterned surface, and thus no wiring to the surface is needed. The assembly of magnetic particles into a chosen pattern of pits using an array of thin-film magnetic elements has recently been demonstrated by Yellen and Friedman.[4]

In the work presented here, thin-film magnetic elements with an elliptical shape were used for the transportation of single magnetic particles. The stray fields created by magnetization of the elements govern the transportation of the particles. The magnetization of the ellipses depends on their geometry and the applied magnetic field. The aspect ratio of an ellipse (the ratio between the long and short axes) determines the magnetic field required to saturate the ellipse along different directions. The magnetic field required to saturate an ellipse along its short axis increases with its aspect ratio.[5] Easily magnetized and demagnetized ellipses are required to enable controlled movement of the magnetic particles. The attractive force from an element on a particle increases with the net magnetization of the element. This allows attachment or detachment of a particle, depending on the magnetization of the element. The distance between a particle and an element is also important since the attractive force decreases with distance.

The magnetic-domain structure was probed by using magnetic force microscopy (MFM). In the MFM images, the contrast indicates the stray fields from the magnetic elements.[6] The MFM images in Figures 1a–d show the magnetic states of 2 μm × 6 μm × 0.1 μm Permalloy ($Fe_{20}Ni_{80}$) ellipses exposed to different in-plane magnetic fields. The elements were fabricated using conventional electron-beam lithography, thermal evaporation, and a lift-off process. The lateral size of the elements is of the same order as the diameter of the particle to avoid more than one particle sticking to each magnetic pole.[7] In zero applied magnetic field (Fig. 1a) symmetric multidomain states appear.[5] In Figures 1b–d, the pattern of elements is exposed to an in-plane magnetic field of constant amplitude (6.3 kA m^{-1}). The direction of the field is indicated by the arrows. The ellipses in the bottom row of Figure 1b, having their long axes parallel to the applied field, are magnetized close to saturation in the direction of the applied field. The ellipses in the top row, having their short axes parallel to the applied field, exhibit non-symmetric multidomain states. Such states imply a weak net magnetization along the field direction. Upon rotating the field to the direction indicated in Figure 1c, the multidomain structure of the top-row elements changes so that the net magnetization along the field direction increases. The bottom-row elements, however, still exhibit a net magnetization close to saturation. This difference is due to their individual magnetic history.[8] The field is rotated further, and, in Figure 1d, the ellipses in the top row are nearly saturated, while the ellipses in the bottom row with their long axis perpendicular to the field exhibit non-symmetric multidomain states. It is important to note that these multidomain states show a net magnetization in the direction of the applied magnetic field. However, their magnetization is significantly weaker than the magnetization of the saturated elements having their long axes parallel to the field.

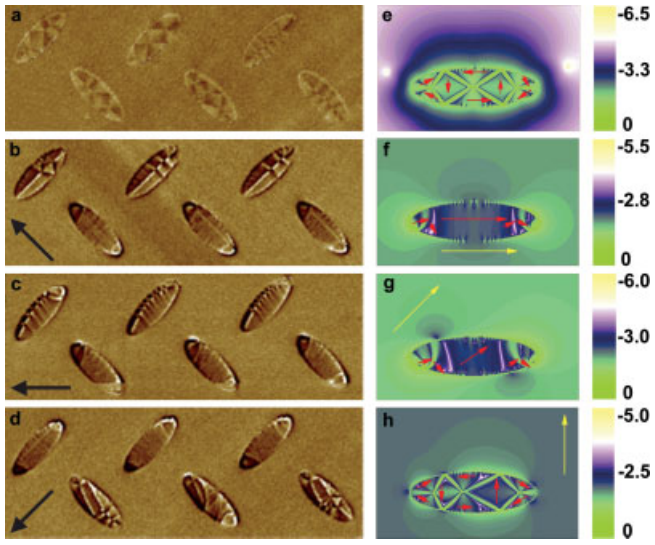

Figure 1. MFM images of the magnetic-domain structures of Permalloy ellipses (2 μm × 6 μm × 0.1 μm) in different applied magnetic fields (left column) and corresponding computer simulations (right column). a) Magnetic-domain structures in zero applied magnetic field. b–d) Arrows indicate the magnetic-field direction of an in-plane field of 6.3 kA m^{-1}. a–d) See text for further information. e–h) Contour plots showing the calculated total effective field inside and the sum of the stray and applied fields outside the elements. The field magnitude is given in units of the saturation magnetization of Permalloy on a logarithmic scale. Magnetization direction within the elements and the applied-field (12.7 kA m^{-1}) direction are indicated by red and yellow arrows, respectively. e) Calculated demagnetized state in zero applied field (cf. a). f) Applied field is parallel to the long axis (cf. bottom-row ellipses in b). g) A nearly saturated ellipse in a field applied 45° to its long axis. The figure also indicates that the net magnetization and stray field of the element follow the rotation of the applied magnetic field (cf. c). h) Applied field is perpendicular to the long axis yielding a non-symmetric multidomain state (cf. top-row ellipses of b). The net magnetization along the field direction for this state is roughly 0.2 of the net magnetization in (f).

To verify the experimental conditions, computer simulations with the object oriented micromagnetic framework (OOMMF) micromagnetic solver were performed.[9] The size of the ellipses was downscaled (due to limitations in computational resources) while keeping the same aspect ratio as used in the experiments. Figure 1e shows a calculated demagnetized state similar to the corresponding experimental state shown in Figure 1a. This state is characterized by a symmetric multidomain structure with net magnetization close to zero. In Figures 1f–h, the ellipse is exposed to a magnetic field of constant amplitude (12.7 kA m^{-1}) in different directions (Figs. 1b–d). As the ellipses are downscaled, the magnitude of the applied magnetic field must be larger in order to imitate the experimental observations.[10] However, the simulations do provide a qualitative description of the experimental conditions. All simulation images are displayed as contour plots, where each color represents the logarithm of the field magnitude, with the magnitude given in units of the saturation mag-

 © 2005 WILEY-VCH Verlag GmbH & Co. KGaA, Weinheim

ADVANCED MATERIALS

netization of Permalloy. In Figure 1f, the ellipse is magnetized close to saturation with the applied field parallel to the long axis. This can be compared to Figure 1h, in which there is only a weak net magnetization when the field is applied along the short axis. The simulations show that the net magnetization of a saturated element is approximately five times stronger than the net magnetization of an element with a non-symmetric multidomain structure (cf. Figs. 1f,h). Since the attractive force exerted by the element on a particle is given by the stray field gradient, a particle will predominantly be attracted to the poles of a saturated element. Nevertheless, there will also be weak attraction of a particle to an element in a non-symmetric multidomain state due to its net magnetization in the direction of the applied field (Fig. 1h).

The magnetic particles used were porous polystyrene spheres with a diameter of 2.8 μm and filled with iron oxide nanoparticles.[11] In these so-called superparamagnetic particles, the direction of the magnetic moment induced by the magnetic field follows the rotation of the external field, and there is no rotation of the particle itself. The magnetic particles were suspended in deionized water, and a certain amount of detergent was added to prevent clustering. The suspension was injected into a system containing a fluid cell and a pump, as shown in Figure 2. A sample containing a pattern of magnetic elements was placed in the fluid cell, visible through an optical microscope. A pair of computer-controlled, perpendicular electromagnets was used to generate a homogeneous magnetic field at the position of the pattern. A weak flow of the suspension was used to trap magnetic particles at the poles of the magnetized elements.

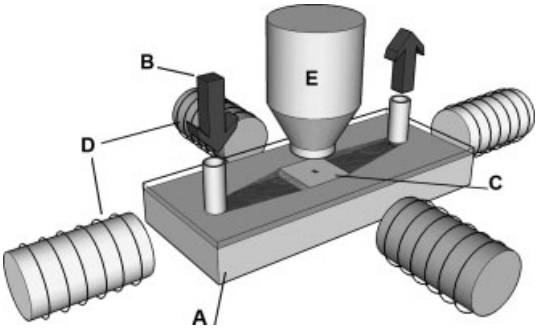

Figure 2. The experimental setup used for controlled movement of magnetic particles consists of a fluid cell (A), a system for injecting particles (B), a sample containing the pattern of magnetic elements (C), two perpendicular iron-core coils producing the magnetic field (D), and an optical microscope to study the movement of the particles (E).

The optical images in Figures 3–5 show how magnetic particles are moved on two specific, patterned magnetic surfaces by using an external, in-plane magnetic field of constant magnitude (6.3 kA m^{-1}) that is stepwise rotated (a few degrees per step). The net magnetization of the elements will therefore rotate in-plane and follow the external magnetic field, as confirmed by the MFM images and the numeric simulations.

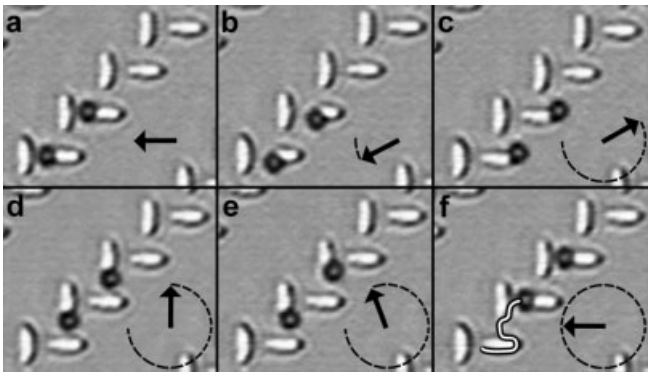

Figure 3. Transportation of magnetic particles in a staircase pattern of magnetic cylindrical ellipses (2 μm × 6 μm × 0.1 μm) in an applied anticlockwise, rotating magnetic field. Due to the rotating magnetic field (6.3 kA m^{-1}), the magnetic-domain structure of the ellipses gradually changes from an almost-saturated state to a non-symmetric multidomain state and back. The arrows indicate the direction of the applied field. The stray fields created by the ellipses follow the applied-field rotation, making the particles follow the ellipse perimeters in the same rotational direction. When the field continues to rotate to the direction shown in (d), the force due to the stray fields of the now nearly saturated vertical ellipses attracts the particles. The field continues to rotate and the particles follow the perimeters of the vertical ellipses (e). After one complete field revolution, the particles have moved one step in the staircase pattern, as shown by the solid curve in (f). See movie in online Supporting Information.

Consequently, the magnetic-domain structure of the ellipses gradually changes from a nearly saturated state (field parallel to the long axis) to a non-symmetric multidomain state (field perpendicular to the long axis), back to a nearly saturated state, and so on. Figure 3 shows two particles moving in a staircase pattern, forming a transport line. The particles move along the perimeter of the ellipses in the rotational direction of the field because they follow the net magnetization of the magnetic elements (Figs. 3b,c). When the field continues to rotate to the direction shown in Figure 3d, the particles are attracted by the stronger stray field from the apex of the now nearly saturated vertical ellipses. Therefore, the particles jump to the neighboring vertical ellipses. After the jump, the particles follow the perimeter of the vertical ellipses anticlockwise as the field continues to rotate anticlockwise. In Figure 3f the field has rotated one complete cycle, and the particles have jumped to the next horizontal elements, which are now close to saturation. This staircase pattern is a one-way transport line; the particles will always jump from the long side of an ellipse (smaller stray fields) to the apex of a neighboring ellipse (larger stray fields) provided that the distance between these two points is short enough. For the pattern discussed in this paper, this is satisfied only for the shortest distance between the long side and the apex of two neighboring ellipses, respectively. This special pattern design allows reliable transportation of particles located at different positions on the transport line. The typical speed of a particle on this pattern can be regulated from a few to tens of micrometers per second by varying the angular frequency of the applied magnetic field.

 © 2005 WILEY-VCH Verlag GmbH & Co. KGaA, Weinheim

The particles follow the perimeters of the ellipses in the same rotational direction as the applied field, i.e., the particles move clockwise or anticlockwise. However, the net displacement of the particles per field revolution is independent of the rotational direction of the field. The benefit of this property is displayed in Figure 4, where junctions are added to the transport line in order to form a loop. The particles are captured in the loop when the field is rotated clockwise (Fig. 4b). If instead the field is rotated anticlockwise (Fig. 4c), the particles will follow the long transport line, ignoring the loop. For the pattern in Figure 4, a magnetic particle can only enter the loop at the second junction (inset of Fig. 4a), because the particle will only jump from an element with a multidomain structure to an almost-saturated element, as described above. This pattern can be utilized for the separation of particles and shows the possibility of constructing junctions where the path of single magnetic particles is programmable by using different field sequences. In Figure 5, two particles trapped in the loop are separated by temporarily changing the rotational direction of the applied field. As the first particle is approaching the second junction, the sense of rotation of the magnetic field is changed to anticlockwise (Fig. 5b). Therefore, the first particle ignores the loop and continues moving along the straight transport line. Changing the rotation of the field back to clockwise keeps the second particle in the loop, and hence, the two particles are separated (Figs. 5c,d).

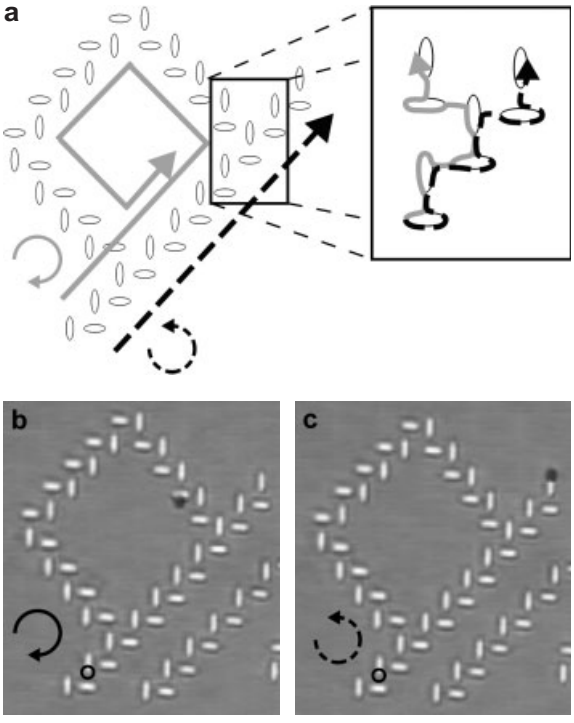

Figure 4. Programmable motion of single magnetic particles. The particles will follow the ellipse perimeters in the rotational direction of the external magnetic field. The arrows in each figure show the sense of field rotation, and the rings in the lower left corners of (b,c) indicate the starting positions of the particles. a) Schematic display of the situation, where the inset indicates the detailed path of the particles at the second junction. b) The particle enters the loop when the field is rotating clockwise. c) The loop is avoided and the particle moves straight on when the field is rotated anticlockwise. See movie in online Supporting Information.

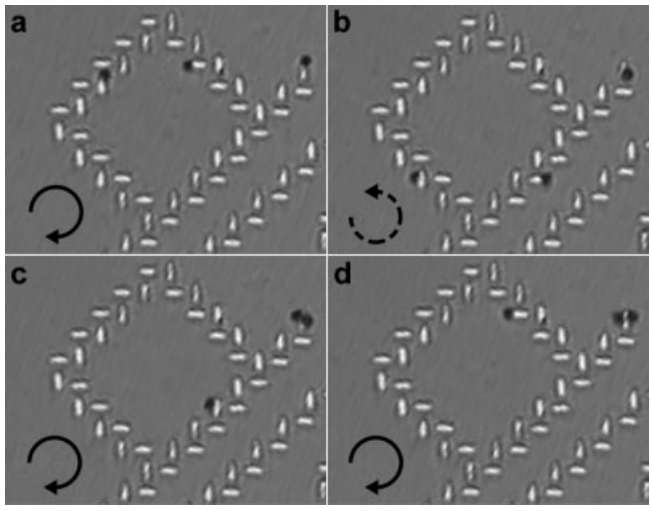

Figure 5. Separation of magnetic particles by changing the rotational direction of the applied magnetic field. The arrows in each figure show the sense of field rotation. a) Two particles are trapped inside the loop. A third particle is located at the end position of the long transport line and is not further considered. b) When the first particle is approaching the second junction, the field rotation is turned anticlockwise. c) The first particle, thus, avoids the loop and continues moving straight to the end of the long transport line. The field is then switched back to clockwise rotation to trap the second particle in the loop. d) The second particle remains in the loop, and the two particles are thus separated. See movie in online Supporting Information.

This work illustrates the feasibility of single magnetic particle transportation and separation using a patterned magnetic surface. Transport lines have been designed where the transportation of particles was controlled by a rotating, external magnetic field. Junctions added to the transport lines allowed programmable movement and separation of particles. A possible way to run many transport systems in parallel would be to combine different designs of elements and transport lines. Potential applications of the method presented here are numerous, for example, in separation, biosensing, and medical diagnostics. Methods for particle detection (e.g., fluorescent labeling) in combination with sophisticated networks consisting of different patterns, such as traps, switches, distributors, and transport lines, could be tailored for lab-on-chip technology.

Experimental

The magnetic structures were created by using electron-beam lithography. The pattern was written in a layer of positive resist on top of a silicon substrate. The Permalloy layer, with a thickness of about 100 nm, was thermally evaporated using a resistively heated tungsten boat. Finally, the resist was removed in a lift-off process, leaving the

 © 2005 WILEY-VCH Verlag GmbH & Co. KGaA, Weinheim

ADVANCED MATERIALS

desired structure of Permalloy elements. The magnetic-domain states of the elements were probed using a Nanoscope Dimension 3100 MFM in lift-mode. The magnetic field was applied in situ by using a specially designed electromagnet integrated in the MFM.

In the computer simulations using the OOMMF [9], a box of dimensions 3 μm × 2 μm, with an ellipse 1.875 μm × 0.625 μm drawn inside, was created. The box was discretized into 5 nm × 5 nm × 31.25 nm blocks with spins placed only within the ellipse, while the area surrounding it was regarded as empty space. The material parameters used were typical for Permalloy (exchange stiffness constant of 13×10^{-12} J m^{-1}, saturation magnetization of 860 kA m^{-1}, and zero magnetocrystalline anisotropy to mimic a polycrystalline sample).

Received: November 16, 2004
Final version: April 1, 2005
Published online: June 7, 2005

[1] a) B. I. Haukanes, C. Kvam, *Bio/Technology* **1993**, *11*, 60. b) R. S. M. S. Karumanchi, S. N. Doddamane, C. Sampangi, P. W. Todd, *Trends Biotechnol.* **2002**, *20*, 72. c) I. Šafařík, M. Šafaříková, *J. Chromatogr. B* **1999**, *722*, 33.
[2] T. Deng, G. M. Whitesides, M. Radhakrishnan, G. Zabov, M. Prentiss, *Appl. Phys. Lett.* **2001**, *78*, 1775.
[3] C. S. Lee, H. Lee, R. M. Westervelt, *Appl. Phys. Lett.* **2001**, *79*, 3308.
[4] B. Yellen, G. Friedman, *Adv. Mater.* **2004**, *16*, 111.
[5] A. Hubert, R. Schäfer, in *Magnetic Domains: The Analysis of Magnetic Microstructures*, Springer, Berlin **1998**, Ch. 5.5.
[6] U. Hartmann, *Annu. Rev. Mater. Sci.* **1999**, *29*, 53.
[7] B. Yellen, G. Friedman, A. Feinerman, *J. Appl. Phys.* **2002**, *91*, 8552.
[8] S. Felton, K. Gunnarsson, P. E. Roy, P. Svedlindh, A. Quist, *J. Magn. Magn. Mater.* **2004**, *280*, 202.
[9] The OOMMF project at the National Institute of Standards and Technology. http://math.nist.gov/oommf/software.html (accessed on April 1, 2005).
[10] M. J. Donahue, D. G. Porter, R. D. McMichael, *J. Appl. Phys.* **2000**, *87*, 5520.
[11] Dynabead M-270 Amine, Dynal Biotech ASA, Oslo (Norway).

An Efficient Solid Oxide Fuel Cell Based upon Single-Phase Perovskites**

By *Shanwen Tao*, *John T. S. Irvine*,* and *John A. Kilner*

Solid oxide fuel cells (SOFCs) promise high efficiencies for a range of fuels. Different oxygen-ion conductors, such as yttria-stabilized zirconia (YSZ),[1] rare-earth-doped ceria,[2] and Sr- and Mg-doped $LaGaO_3$ (LSGM)[3] have been investigated as electrolytes for SOFCs. Doped ceria exhibits significant electronic conductivity above 600 °C, which limits its application as an electrolyte above this temperature. At lower temperatures, the electrode process is typically rather slow, which may increase the overpotential across the electrode. LSGM exhibits higher conductivity than YSZ at higher temperatures, which makes it easier to achieve higher power density if suitable electrode materials are utilized. Cobalt doping (i.e., to make LSGMCo) is reported to increase conductivity even further, and if kept at a fairly low level, does not induce significant electronic conductivity.[4,5] Unlike gadolinia-doped ceria (CGO) and YSZ that exhibit fluorite structure, LSGM and LSGMCo have a perovskite structure. Many perovskite oxides such as Sr-doped $LaMO_3$ (M = Mn, Fe, Co, or Ni) exhibit very high p-type electronic or mixed-oxide ionic electronic conductivity at elevated temperatures.[6–9] These perovskite oxides, particularly Sr-doped $LaCoO_3$, exhibit very high conductivity (up to 1000 S cm^{-1} at 1000 °C for $La_{0.8}Sr_{0.2}CoO_3$) and are good cathode materials for SOFCs. The perovskite oxide $La_{0.6}Sr_{0.4}CoO_3$ has been demonstrated as a very good cathode material for SOFCs when LSGM is used as the electrolyte.[3,10] The conventional anode for SOFCs, the Ni(O) cermet, is known to react with LSGM with major NiO diffusion through the electrolyte on fabrication.[11,12] The poor redox stability of these cermets may cause cracking during cycling of the fuel cell. The cermet anode and then the whole stack may be damaged if any air is introduced into the anode owing to leaking. It is hoped that these problems may be overcome by the use of a redox-stable anode. Thus, an alternative anode material would be of considerable benefit. In addition, polarization losses at the interfaces between electrolyte and electrode may be minimized if we can use only perovskite oxides as the main components of a fuel cell. For these reasons, a good perovskite anode is in demand for this type of SOFC. However, most conductive perovskite oxides are unstable in a reducing environment at high temperature. Recently we found that $(La_{0.75}Sr_{0.25})Cr_{0.5}Mn_{0.5}O_{3-\delta}$ (LSCM) is a good redox-stable perovskite anode for SOFCs when YSZ is used as the electrolyte.[13–15] Furthermore, it is interesting to note that the primitive perovskite unit-cell volume of as-prepared $(La_{0.75}Sr_{0.25})_{0.95}Cr_{0.5}Mn_{0.5}O_{3-\delta}$ is 58.09 Å^3, changing to 59.05 Å^3 on reduction.[15] This matches very well with the primitive cell volume of LSGM, which is 59.55 Å^3.[16] Table 1 lists the room-temperature lattice parameters, reduced lattice volume, and space group of some perovskite oxides for comparison. The thermal expansion coefficients for $La_{0.9}Sr_{0.1}Ga_{0.8}Mg_{0.2}O_{3-\delta}$ and LSCM are 11.5×10^{-6} K^{-1} and 9.3×10^{-6} K^{-1}, respectively, which are also quite close.[15,17] This makes it possible to design an all-perovskite fuel cell using LSCM as the anode and LSGM or LSGMCo as the electrolyte. Clearly there are many perovskite cathodes that could be utilized in an all-perovskite fuel cell. In this study we decided to use $Gd_{0.4}Sr_{0.6}CoO_{3-\delta}$ as it has recently been shown to yield good performance with gadolinia ceria electrolytes.[18] The primitive unit-cell volume of $Gd_{0.5}Sr_{0.5}CoO_{3-\delta}$ is only 55.08 Å^3 and its thermal expansion coefficient would be expected to be in

[*] Prof. J. T. S. Irvine, Dr. S. W. Tao
School of Chemistry, University of St Andrews
Fife KY16 9ST, Scotland (UK)
E-mail: jtsi@st-andrews.ac.uk
Prof. J. A. Kilner
Department of Materials, Imperial College
London SW7 2BP (UK)

[**] We thank EPSRC and NEDO (All Perovskite Solid Oxide Fuel Cell) for support and Sylvia Williamson for assistance with ICP-MS analysis.

 © 2005 WILEY-VCH Verlag GmbH & Co. KGaA, Weinheim DOI: 10.1002/adma.200402007